28. W. Ma, C. Yang, X. Gong, K. Lee, A. J. Heeger, *Adv. Funct. Mater.* **15**, 1617–1622 (2005).
29. S. Cook, R. Katoh, A. Furube, *J. Phys. Chem. C* **113**, 2547–2552 (2009).
30. J. Clark, C. Silva, R. H. Friend, F. C. Spano, *Phys. Rev. Lett.* **98**, 206406 (2007).
31. W. J. D. Beenken *et al.*, *Phys. Chem. Chem. Phys.* **15**, 16494–16502 (2013).
32. C. Manzoni, D. Polli, G. Cerullo, *Rev. Sci. Instrum.* **77**, 023103 (2006).
33. W. J. Grzegorczyk *et al.*, *J. Phys. Chem. C* **114**, 5182–5186 (2010).
34. P. J. Brown *et al.*, *Phys. Rev. B* **67**, 064203 (2003).
35. D. S. Bethune, G. Meijer, W. C. Tang, H. J. Rosen, *Chem. Phys. Lett.* **174**, 219–222 (1990).
36. S. Falke, P. Eravuchira, A. Materny, C. Lienau, *J. Raman Spectrosc.* **42**, 1897–1900 (2011).
37. X. Andrade *et al.*, *J. Chem. Theory Comput.* **5**, 728–742 (2009).
38. A. Castro *et al.*, *Phys. Status Solidi B Basic Res.* **243**, 2465–2488 (2006).

ACKNOWLEDGMENTS

Financial support by the European Union project CRONOS (grant number 280879-2), the Deutsche Forschungsgemeinschaft (SPP1391), the Korea Foundation for International Cooperation of Science and Technology (Global Research Laboratory project, K20815000003), and the Italian Fondo per gli Investimenti della Ricerca di Base (Flashit project) is gratefully acknowledged. C.A.R. and E.M. acknowledge the Partnership for Advanced Computing in Europe (project LAIT) for awarding us access to supercomputing resources at CINECA, Italy, and useful discussions with C. Cocchi and Y. Kanai. S.M.F. is grateful for a Ph.D. fellowship from Stiftung der Metallindustrie im Nord-Westen. C.L. and G.C. acknowledge support from the European Community (Seventh Framework Programme INFRASTRUCTURES-2008-1, Laserlab Europe II contract no. 228334); A.R. acknowledges financial support from the European Research Council (ERC-2010-AdG-267374), Spanish grant (FIS2010-21282-C02-01), Grupos Consolidados (IT578-13), Ikerbasque. G.C. acknowledges financial support by the European Research Council (ERC-2011-AdG no. 291198). C.L., S.M.F., G.C., C.A.R., and E.M. initiated this work. S.M.F. prepared the samples. S.M.F., D.B., M.M., E.S., and A.D.S. performed the ultrafast spectroscopy experiments. C.A.R. and M.A. performed DFT and TDDFT simulations. S.M.F., A.D.S., D.B., G.C., and C.L. analyzed and discussed the experimental data. C.A.R., M.A., E.M., and A.R. analyzed and discussed the theoretical data. C.A.R., E.M., G.C., A.D.S., and C.L. designed the paper. All authors discussed the implications and contributed to the writing of the paper. The authors declare no competing financial interests.

SUPPLEMENTARY MATERIALS

www.sciencemag.org/content/344/6187/1001/suppl/DC1
Materials and Methods
Supplementary Text
Figs. S1 to S10
References (*39*–*48*)
Movies S1 and S2

16 December 2013; accepted 7 May 2014
10.1126/science.1249771

WATER SPLITTING

Amorphous TiO_2 coatings stabilize Si, GaAs, and GaP photoanodes for efficient water oxidation

Shu Hu,[1,2] Matthew R. Shaner,[1,2] Joseph A. Beardslee,[1] Michael Lichterman,[1,2] Bruce S. Brunschwig,[3] Nathan S. Lewis[1,2,3,4]*

Although semiconductors such as silicon (Si), gallium arsenide (GaAs), and gallium phosphide (GaP) have band gaps that make them efficient photoanodes for solar fuel production, these materials are unstable in aqueous media. We show that TiO_2 coatings (4 to 143 nanometers thick) grown by atomic layer deposition prevent corrosion, have electronic defects that promote hole conduction, and are sufficiently transparent to reach the light-limited performance of protected semiconductors. In conjunction with a thin layer or islands of Ni oxide electrocatalysts, Si photoanodes exhibited continuous oxidation of 1.0 molar aqueous KOH to O_2 for more than 100 hours at photocurrent densities of >30 milliamperes per square centimeter and ~100% Faradaic efficiency. TiO_2-coated GaAs and GaP photoelectrodes exhibited photovoltages of 0.81 and 0.59 V and light-limiting photocurrent densities of 14.3 and 3.4 milliamperes per square centimeter, respectively, for water oxidation.

The oxidation of water to O_2 is a key process in the direct photoelectrochemical (PEC) production of fuels from sunlight (*1*, *2*). A fuel-forming reductive half-reaction involving the reduction of CO_2 to lower hydrocarbons or the reduction of H_2O to H_2 requires an oxidative half-reaction, such as the oxidation of water to O_2. Metal oxide photoanodes can oxidize water to O_2 in alkaline or acidic media, but thus far have been inefficient because their band gaps are too large and because the potential of their valence band edge is much more positive than the formal potential for water oxidation, $E^{o'}(O_2/H_2O)$ (*3*). Although many semiconductors, including silicon (Si), gallium arsenide (GaAs), and gallium phosphide (GaP), have valence-band edges at more negative potentials than metal oxides and also typically have optimal band gaps for efficient solar-driven water splitting, these semiconductors are unstable when operated under photoanodic conditions in aqueous electrolytes. Specifically, in competition with oxidizing water to O_2, these materials either anodically photocorrode or photopassivate (*3*, *4*). Furthermore, passive and intrinsically safe solar-driven water-splitting systems can only be constructed (*5*) in either alkaline or acidic media, and the development of general strategies to stabilize existing photoelectrode materials under water-oxidation conditions is an important goal.

Various coating strategies have been explored to stabilize semiconductors with optimal band gaps (1.1 to 1.7 eV) for direct water splitting (*6*). Deposition of thin films of Pd (*7*), Pt (*8*), Ni (*9*), or metal-doped SiO_x (*10*) onto n-type Si or n-GaAs photoanodes yields improved stability under water-oxidation conditions, primarily near neutral pH, as well as in strongly alkaline (*9*) or acidic (*10*) media for up to 12 hours. However, these stabilized photoanodes generally exhibit low photovoltages; additionally, the protective metal coating is either too thick to be highly optically transmissive or too thin to afford extended stability during water oxidation, particularly in alkaline or acidic media. Transparent conductive oxide (TCO) coatings on Si and GaAs are not stable in strongly alkaline or acidic media, and also produce low voltages because of defective semiconductor/TCO interfaces. (*11*, *12*) Coatings of Ni islands (*9*), as well as MnO_x (*13*) and NiO_x (*14*) films on Si, have been used to catalyze the oxidation of water and thus provide some degree of stability enhancement. However, such coatings do not enable prolonged operation in alkaline media and/or yield very low photovoltages because of a large density of interface states at the Si/Ni interface.

Conformal layers of 2-nm thin TiO_2 formed by atomic layer deposition (ALD) have been used to stabilize Si, and in conjunction with an IrO_x catalyst, to effect water oxidation (*15*). Deposition of such electrically insulating films at larger thickness, to reliably prevent pinholes and thus suppress active corrosion over macroscopic areas, creates a tunneling barrier for photogenerated holes. As this barrier becomes thicker, it no longer conducts holes via a tunneling mechanism and also introduces a large series resistance to a PEC device, degrading its efficiency to low values. Specifically, as the TiO_2 thickness was increased, the overpotential for the oxygen-evolution reaction (OER) increased linearly at a rate of ~21 mV nm^{-1} (*16*), resulting in an additional voltage loss of ~200 mV for a 12-nm thick TiO_2 overlayer, even at a current density of 1 mA cm^{-2}.

We describe a general approach to significantly improve the stability of Si, GaAs, and GaP photoanodes against both photocorrosion and photopassivation for water oxidation in alkaline media [all results reported below are

---

[1] Division of Chemistry and Chemical Engineering, California Institute of Technology, Pasadena, CA 91125, USA. [2] Joint Center for Artificial Photosynthesis, California Institute of Technology, Pasadena, CA 91125, USA. [3] Beckman Institute and Molecular Materials Research Center, California Institute of Technology, Pasadena, CA 91125, USA. [4] Kavli Nanoscience Institute, California Institute of Technology, Pasadena, CA 91125, USA.
*Corresponding author. E-mail: nslewis@caltech.edu

for 1.0 M aqueous KOH (pH 13.7) unless noted otherwise]. Instead of promoting corrosion of the underlying anode, the photogenerated holes are conducted away from the semiconductor through hundred-nanometer-thick, "electronically leaky" TiO_2 films to Ni islands on the surface of the film, where the holes are used by Ni oxide to oxidize water to O_2 (Fig. 1A). The Ni islands or thin Ni film/TiO_2 coating transmits most of the incident light and preserves high short-circuit photocurrent densities expected from the underlying semiconductor under simulated sunlight. The conduction mechanism through the protective coating is different from that obtained from a tunneling barrier, and the photoanodes additionally exhibited much larger photovoltages than those obtained from the direct deposition of metal or TCO films onto Si or GaAs photoanodes (*6*, *7*, *10*, *11*).

Thick overlayers of TiO_2 (4 to 143 nm) were deposited on Si, GaAs, and GaP electrodes by ALD, to provide a range of coating thicknesses that allowed for minimization of the pinhole density while providing conformality and acceptable barrier layer properties. Thermal annealing produced stoichiometric insulating crystalline TiO_2 films that created an interfacial tunneling barrier for photogenerated charge carriers. Hence, instead we used unannealed TiO_2, which is electronically defective and possibly nonstoichiometric, to allow for the passage of very high (>1 A cm^{-2}) current densities as a "leaky" dielectric (*17*). The electronic defects in these unannealed ALD-grown TiO_2 films presumably arise from structural disorder (amorphous phase) and/or chemical impurities (such as carbon or nitrogen) from the precursors used in the ALD process [as shown by secondary-ion mass spectroscopy, fig. S1 (*18*)]. Hall measurements indicated that the concentration of electrons in the as-grown ALD-TiO_2 was 4×10^{16} cm^{-3}. We then deposited a 100-nm-thick Ni film or 100-nm-thick Ni islands (square arrays of 3-μm-diameter circles on a 7-μm pitch) onto the TiO_2 overlayer by sputtering or electron-beam evaporation.

The electrochemical current density (*J*) versus potential (*E*) behavior of degenerately p-type doped p^+-Si and p^+-GaAs electrodes covered with 4 to 143 nm of TiO_2 and a 100-nm-thick Ni film were measured in the dark to determine the overpotential associated with these films. The catalytic activity of Ni oxide improves over time in alkaline electrolytes, and hence the depicted data are from the third voltammetric cycle of the electrode. The overpotential required to drive the OER at a current density of 10 mA cm^{-2} was 0.34 to 0.37 V for a degenerately doped p^+-Si/TiO_2/Ni-film electrode and was 0.37 V for a p^+-GaAs/TiO_2/Ni-film electrode [fig. S2 (*18*)]. At a current density of 20 mA cm^{-2}, the voltage loss caused by the TiO_2 coatings on a p^+-Si/TiO_2/Ni-film electrode was thus <50 mV as compared to that of a continuous 100–nm-thick Ni film with no intervening TiO_2 layer. The measured overpotentials are in accord with the reported behavior of Ni oxide for OER in alkaline media. (*19*–*21*) An oxygen probe indicated that O_2 (gaseous) was produced with 99 ± 1% Faradaic efficiency in these systems.

The PEC behavior of unannealed TiO_2 coatings on photoactive n-Si and n-GaP, as well as the behavior of unannealed TiO_2 on buried-junction n-p^+-Si photoelectrodes and on buried-junction n-p^+-GaAs electrodes, is shown in Fig. 1, B to E. The electrocatalyst overlayers were 100-nm-thick patterned Ni islands on Si and were 2-nm Ni films on GaAs and GaP. A p^+ emitter layer was additionally formed on the n-Si to demonstrate

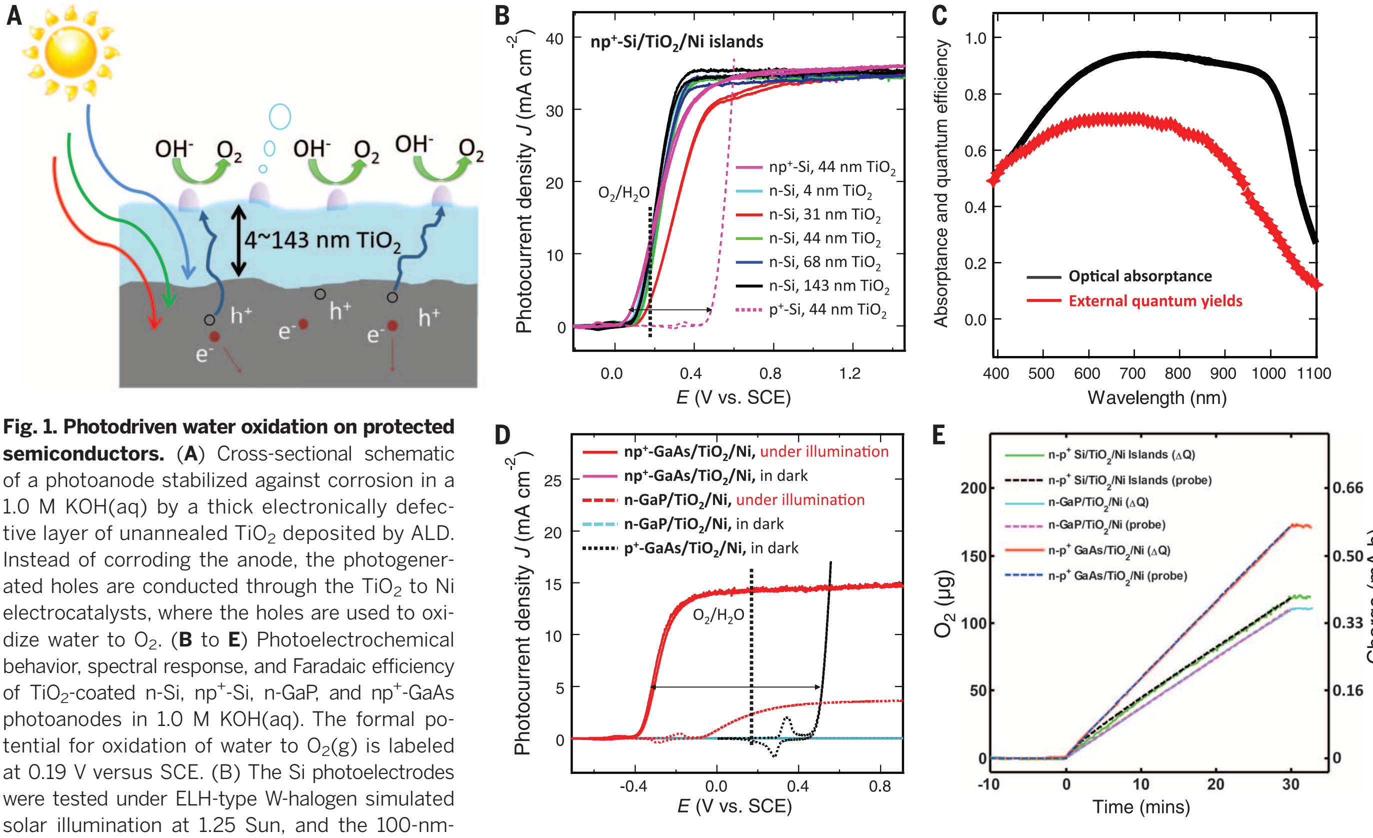

Fig. 1. Photodriven water oxidation on protected semiconductors. (**A**) Cross-sectional schematic of a photoanode stabilized against corrosion in a 1.0 M KOH(aq) by a thick electronically defective layer of unannealed TiO_2 deposited by ALD. Instead of corroding the anode, the photogenerated holes are conducted through the TiO_2 to Ni electrocatalysts, where the holes are used to oxidize water to O_2. (**B** to **E**) Photoelectrochemical behavior, spectral response, and Faradaic efficiency of TiO_2-coated n-Si, np^+-Si, n-GaP, and np^+-GaAs photoanodes in 1.0 M KOH(aq). The formal potential for oxidation of water to O_2(g) is labeled at 0.19 V versus SCE. (B) The Si photoelectrodes were tested under ELH-type W-halogen simulated solar illumination at 1.25 Sun, and the 100-nm-thick Ni-island electrocatalysts were patterned in square arrays of 3-μm-diameter circles on a 7-μm pitch. (**C**) Overlay of the normal-incidence optical absorptance and external quantum yields for n-Si photoelectrodes coated with 68 nm of TiO_2 and patterned Ni islands. The electrode potential was held at 0.35 V versus SCE. (**D**) The 2-nm Ni /118-nm TiO_2–coated np^+-GaAs and n-GaP photoelectrodes were tested under simulated AM 1.5 illumination at 1 Sun and in the dark. The dark behavior of typical p^+-Si/TiO_2/Ni and p^+-GaAs/TiO_2/Ni electrodes is chosen from fig. S2 (*18*) and included in (B) and (D), respectively, to show the shift in potential of the photoelectrodes. (**E**) Overlay of the cumulative O_2(g) detected and charge passed from 0 to 30 min for Ni islands/44-nm TiO_2-coated np^+-Si and np^+-GaAs photoelectrodes, and 2-nm Ni/118-nm TiO_2-coated n-GaP photoelectrodes. The electrodes were held at 0.05, −0.32. and 0.18 V versus SCE, respectively. The axes were labeled assuming a 100% Faradaic efficiency when the data for charge passed and O_2 detected overlap.

the versatility of the protection strategy, because this buried junction was expected to produce a characteristic open-circuit voltage, V_{oc}, of 0.50 to 0.55 V at illumination intensities sufficient to produce short-circuit photocurrent densities of 33.6 mA cm^{-2}, in accord with expectations based on the diode-limited performance of Si n-p$^+$ junctions at the doping densities investigated.

Under 1.25-Sun of ELH-type W-halogen simulated solar illumination, the light-limited photocurrent density of the n-Si/TiO_2/Ni-island and n-p$^+$-Si/TiO_2/Ni-island electrodes was 34.7 ± 1.7 mA cm^{-2} for a TiO_2 thickness of 4 to 143 nm (Fig. 2A), corresponding to a photocurrent density of 27.7 ± 1.4 mA cm^{-2} at 1 Sun. This current density is in accord with expectations (27.0 mA cm^{-2}) based on an integration of the measured spectral response of the photoanodes (Fig. 2B) with the air mass (AM) 1.5 1-Sun solar spectrum. The n-p$^+$-Si/TiO_2/Ni-island and n-p$^+$-GaAs/TiO_2/Ni-film photoanodes exhibited photovoltages of 0.52 ± 0.03 V and 0.81 ± 0.02 V relative to the formal potential for water oxidation, $E^{o\prime}(O_2/H_2O)$ of 0.19 V versus a saturated calomel electrode (SCE), respectively. Under the respective illumination conditions, the Si/TiO_2/Ni island photoelectrode exhibited a photocurrent density of 6.6 mA cm^{-2} at a potential of 0.13 V versus SCE, and the GaAs/TiO_2/Ni film photoelectrode exhibited a photocurrent density of 11.9 mA cm^{-2} at a potential of –0.22 V versus SCE. The n-GaP/TiO_2/Ni film photoanodes showed a 0.59 ± 0.02 V photovoltage versus $E^{o\prime}(O_2/H_2O)$ under simulated AM 1.5 1-Sun illumination, with a photocurrent density of 1.4 mA cm^{-2} at a potential of 0.06 V versus SCE. The light-limited photocurrent densities for the TiO_2-coated GaAs and GaP photoelectrodes were 14.3 and 3.4 mA cm^{-2} at 1 Sun, respectively. The catalytic currents for Si, GaAs, and GaP photoanodes became significant on this current scale at ~0.3 V more positive than the measured open-circuit potentials of the respective photoelectrodes under illumination, due to the overpotentials associated with electrocatalysis of the OER under these conditions. The O_2(g) detected by an O_2 probe (Fig. 1E) was plotted assuming that four holes generated one molecule of O_2(g) at 100% Faradaic efficiency; i.e., 0.33 mA hour of charge passed corresponded to 100 μg of generated O_2. All of these photoelectrodes thus showed 99 ± 1% Faradaic efficiency for O_2 production, as determined by the calibrated O_2 probe.

Figure 2 shows the photocurrent density as a function of time for an n-p$^+$-Si/TiO_2/Ni-island electrode under light-limited conditions (1.25 Sun) at 0.93 V versus SCE. The light intensity was monitored by a photodiode, and fluctuations of the photocurrent were caused by the formation of O_2 bubbles on the electrode as well as by variations in the illumination intensity from the lamp. The photocurrent for the unannealed, electronically defective TiO_2-coated Si photoelectrode with patterned Ni islands decreased by ~10% after 100 hours of continuous operation, and the fill factor (*ff*) decreased only slightly [<5%; fig. S5 (*18*)]. The analogous n-p$^+$-GaAs/TiO_2/Ni-film and n-GaP/TiO_2/Ni-film photoanodes also exhibited stable water-oxidation photocurrents for >25 hours of continuous operation [fig. S6 (*18*)]. The photocurrent and *ff* decreased by ~8% and <5% after 5 hours, respectively.

Fig. 2. Chronoamperometry of an n-p$^+$-Si photoanode coated with 44 nm of TiO_2 and Ni islands for over 100 hours in 1.0 M KOH(aq). The photocurrent density versus time (red curve) was overlaid with the illumination intensity versus time (black curve). The electrode potential was held at 0.93 V versus SCE. The ENH-type tungsten-halogen light bulb burned out at the 54th hour and was then replaced with another ENH bulb, and the experiment was continued as indicated. The illumination intensity was 1.25 Sun.

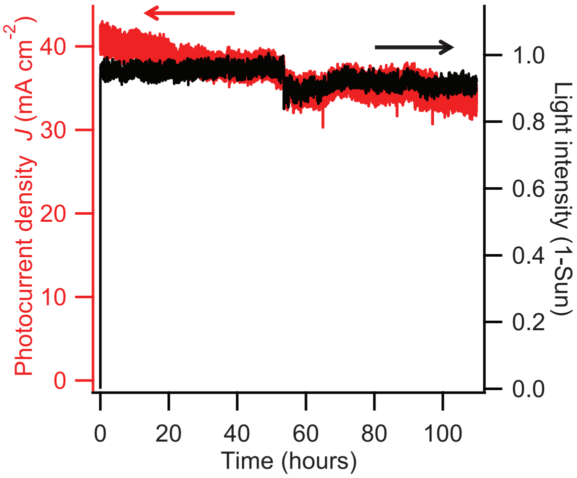

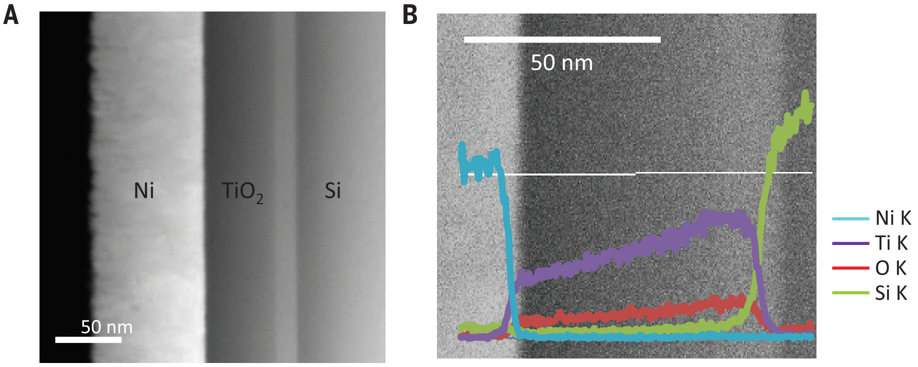

Fig. 3. Structural and chemical characterization of the Si/TiO_2/Ni interface. Both Ni and TiO_2 films in this study were continuous, with thicknesses of 100 nm and 68 nm, respectively. (**A**) Elemental contrast image of the Si/TiO_2/Ni interface by scanning TEM. (**B**) EDS line profiles of Ni, Ti, O, and Si across the TiO_2 interface.

The Si/TiO_2/Ni interface was characterized in cross-section using element-contrast scanning transmission electron microscopy (Fig. 3A) as well as energy-dispersive x-ray spectroscopy (EDS) with <1 nm spatial resolution (Fig. 3B). The EDS line profiles of Ni, Ti, and O across the same TiO_2/Ni interface showed a gradual decrease of the Ni signal as the Ti signal increased when the sampled area was scanned from the bulk Ni film into the TiO_2 film. Hence, detectable intermixing of Ni and TiO_2 occurred only within a region ~5 nm in depth. The major diffraction-ring pattern observed in a selected-area diffraction pattern acquired at the Ni/TiO_2 interface indicated the presence of a polycrystalline phase of Ni, whereas the diffused ring that surrounded the transmitted beam can be attributed to the amorphous structure of the TiO_2 [fig. S7 (*18*)].

Secondary-ion mass spectrometry (SIMS) on TiO_2 films with and without Ni deposition [fig. S1 (*18*)] confirmed the EDS results. The SIMS data also indicated that the deposited Ni did not penetrate through the full 143-nm depth of TiO_2. Specifically, no Ni filaments extending through the film were detected either from the SIMS data on a 125 × 125 μm^2 area of the TiO_2 sample or by the TEM characterization within ~10 μm width of the thin region.

Figure 4 shows the behavior of Si/TiO_2/Ni film or Ni-island electrodes in contact with an aqueous solution of the one-electron, outer-sphere, reversible, $Fe(CN)_6^{3-/4-}$ (50 mM/ 350 mM) redox couple. Mass transport–limited anodic current densities of 120 mA cm^{-2} were observed for p$^+$-Si/TiO_2/Ni-film electrodes in the dark (Fig. 4A), and light-limited anodic current densities of 35 mA cm^{-2} were observed for n-Si/TiO_2/Ni-island electrodes under illumination (Fig. 4B). These results indicate that holes were readily conducted through the TiO_2 overlayer to the $Fe(CN)_6^{3-/4-}$ redox couple in the presence of Ni films or Ni islands on the TiO_2 surface. For comparison, Fig. 4A displays the behavior of a continuous Ni film electrode tested under the same conditions (orange curve). The p$^+$-Si/TiO_2/Ni-film and the Ni film electrodes showed mutually similar resistances near the rest potential of 0.19 V versus SCE. The upper and lower limits of each data set in Fig. 4A are indicative of the limiting anodic and cathodic current densities, respectfully, and result from diffusion and convection of redox species in an agitated solution. The same behavior was also observed in the dark for p^+-GaAs/68-nm TiO_2/Ni electrodes [fig. S8 (*18*)].

Under simulated 1.25-Sun illumination, an n-Si/TiO_2/Ni-island electrode in contact with the $Fe(CN)_6^{3-/4-}$ redox couple exhibited V_{oc} = 0.41 ± 0.03 V [versus the $Fe(CN)_6^{3-/4-}$ Nernstian cell potential] and light-limited photocurrent densities of 34.6 ± 0.6 mA cm^{-2} (Fig. 4B). A *ff* of 0.49 ± 0.08 was calculated at the maximum power-conversion point, with the V_{oc} defined as the potential difference between the n-Si/TiO_2/Ni-island photoanode under illumination and the Nernstian potential of the $Fe(CN)_6^{3-/4-}$ solution. The light-limited photocurrent densities in contact with $Fe(CN)_6^{3-/4-}$(aq) were within ± 2 mA cm^{-2} of those observed for the same electrodes during the OER in contact with 1.0 M KOH(aq).

The data indicate that the unannealed ALD-TiO_2 films prepared and exploited in our work are "leaky" (electronically defective) and thus highly conductive, with the exception of a thin insulating barrier layer at the surface of the as-grown film. In this model, intermixing of the deposited Ni provides electrical contact through the insulating surface layer. This combination allowed the thick ALD-TiO_2 films to act as a highly effective corrosion barrier while facilitating interfacial charge transport with minimal resistive loss. Consistently, without a Ni film or Ni islands, rectifying *J-E* behavior and low anodic current densities were observed for p^+-Si/TiO_2 electrodes in the dark and for n-Si/TiO_2 under illumination. This hypothesis is also consistent with the behavior observed in contact with $Fe(CN)_6^{3-/4-}$(aq) [fig. S9 (*18*)] and 1.0 M KOH(aq) [fig. S10 (*18*)]. When the ALD-TiO_2 surface was sputtered to remove the top layer and left with trace metals on the surface [fig. S11 (*18*)], the TiO_2 film exhibited anodic current densities of >120 mA cm^{-2} in contact with $Fe(CN)_6^{3-/4-}$(aq). Furthermore, when a Hg drop was used to contact p^+-Si/unannealed TiO_2 samples, anodic current densities of <0.2 μA cm^{-2} were measured at a 0.02 V bias voltage, whereas the Hg-drop–contacted samples passed >10^4 larger anodic current densities at this bias when the top layer of the ALD-TiO_2 films was either intermixed with Ni or was removed physically [fig. S12 (*18*)]. Ir deposits also enabled anodic conduction through the unannealed TiO_2 films, but the observation of anodic current densities of 50 to 120 mA cm^{-2} required additional voltage losses of ~0.40 V when Ir was used instead of Ni.

The observed energy-band alignment for a p^+-Si substrate with an ALD-grown unannealed TiO_2 film indicated a large valence-band offset of 2.22 ± 0.08 eV [fig. S13 (*18*)]. The potential distribution under operation is expected to be a complicated function of the energetics and charge-transfer kinetics at the various interfaces in these multicomponent photoelectrode systems. Spectroscopic ellipsometry data indicated that the optical band gap for the TiO_2 film was 3.34 ± 0.01 eV [fig. S14 (*18*)]. Unlike photocathodes, where electrons can be expected to inject into the conduction band of TiO_2 (*22*), stoichiometric nondefective TiO_2 films should present a tunneling barrier for holes in the valence band. Hence, TiO_2 films with thicknesses of 4 to 143 nm should attenuate anodic currents to levels at or below 100 μA cm^{-2}, in accord with prior observations (*23*, *24*). A Mott-Schottky analysis indicated that the flat-band potential of TiO_2 in contact with $Fe(CN)_6^{3-/4-}$(aq) was –1.4 V versus SCE [fig. S15 (*18*)]. However, x-ray photoemission spectra revealed a 2-eV-wide distribution of filled defect states spanning from the conduction band to the mid-gap region (Fig. 4C), suggesting that holes could be transported through TiO_2 preferentially via the defect states instead of by the valence band. These defect states are not present, presumably due to oxidation by air or water, at the TiO_2 surface after the ALD process. This hypothesis is consistent with the observation that invasive contacts, established by Ni intermixing or physical removal of the most exposed layer of the TiO_2 film, enabled conduction pathways via these defect states, whereas nonpenetrating contacts such as the Hg drop or an aqueous redox solution did not effectively access these defect states and thus exhibited minimal conduction through the entire unannealed TiO_2 thick overlayer.

Consistently, relatively large cathodic current densities, >15 mA cm^{-2}, were observed for TiO_2-coated Si and GaAs, even without a thin metallic film deposited on the TiO_2 surface (Fig. 4 and fig. S10). The 0.0 ± 0.1 eV conduction band offset for Si and TiO_2 suggests a band-transport mechanism for electron conduction. Three- to 100-nm-thick TiO_2 coatings have been shown to protect photocathodes of p-InP (*25*), p-Cu_2O/n-ZnO (*26*), and p-Si (*27*) by allowing electrons to transport via the conduction band of TiO_2 and are normally designed to block hole transport (*28*).

The key to enabling the conduction of holes across the thick TiO_2 protective coating is the use of unannealed ALD-TiO_2. Unannealed ALD TiO_2 combines optical transparency and high electrical conductivity to both electrons and holes, while allowing the incorporation of metal catalyst overlayers and providing chemical stability in a variety of aqueous media, specifically including alkaline anodic operational conditions. Because defect states (0 to 2 eV versus the conduction-band edge) exist in the ALD-TiO_2 film (Fig. 4C), the observed hole conduction exhibited negligible voltage loss and was independent of film thickness over the range of 4 to 143 nm. When the TiO_2 film was annealed, the observed anodic current densities decreased to 2 mA cm^{-2} at 0.50 V overpotential versus $Fe(CN)_6^{3-/4-}$(aq), even when a Ni overlayer was deposited on top of 4 nm of ALD-TiO_2 [fig. S16 (*18*)].

For the n-p^+-Si/TiO_2/Ni-island photoanode, the photovoltage from the Si mainly offset the overpotential for water oxidation for this

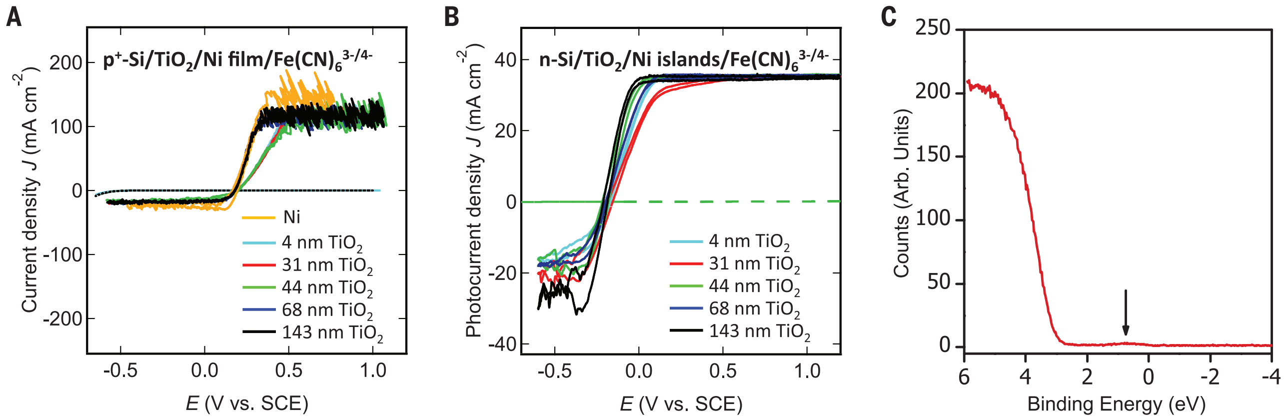

Fig. 4. Defect-state–mediated hole-conduction mechanism. (**A**) Electrochemical behavior of p^+-Si/TiO_2/Ni-film electrodes in contact with 50 mM $Fe(CN)_6^{3-}$ and 350 mM $Fe(CN)_6^{4-}$(aq) in the dark. The dashed curves indicate the behavior without Ni; i.e., p^+-Si/3-nm and 143-nm TiO_2 [all thicknesses are shown in fig. S10 (*18*)]. (**B**) PEC behavior of n-Si/TiO_2/Ni island photoelectrodes in the same electrolyte under simulated ELH-type 1.25-Sun illumination. The dashed curve indicates the behavior of n-Si/44-nm TiO_2 photoelectrodes without Ni. The Nernstian potential of the $Fe(CN)_6^{3-/4-}$ solution was 0.19 V versus SCE. Ni films were deposited for TiO_2-coated p^+-Si, whereas Ni islands (square arrays of 3-μm-diameter circles in 7-μm pitch) were deposited on TiO_2-coated n-Si. (**C**) X-ray photoemission valence spectrum of the 44-nm ALD-TiO_2 on Si without removing the top layer of the nonconducting TiO_2, indicating the filled defect states in the TiO_2 band gap.

state-of-the-art electrolyte/electrocatalyst combination (*29*). The *J-E* data for this photoanode thus extended only slightly into the power-producing region; i.e., anodic photocurrents of ~10 mA cm^{-2} were observed at negative electrode potentials relative to $E^{o\prime}(O_2/H_2O)$. Nevertheless, to provide perspective on the shift in potential provided by the photoelectrode, obtaining the observed *J-E* performance of the n-p$^+$-Si/44-nm TiO_2/Ni island photoanode with a Si photovoltaic (PV) cell electrically in series with an electrocatalytic anode that exhibited identical *J-E* behavior to that of the p$^+$-Si/44-nm TiO_2/Ni film electrode in the dark (*30*) would require the use of a 9.4% efficient Si PV cell with a V_{oc} of 0.43 V, a J_{sc} (short-circuit photocurrent density) of 27.7 mA cm^{-2}, and a *ff* of 0.79. In fact, the required 9.4% PV energy-conversion efficiency is an underestimation of the light-induced performance of the photoelectrode, because the light-blocking electrocatalytic Ni islands covered 14.4% of the electrode surface, and thus an ~11.0% efficient PV cell connected in series with the electrocatalyst/electrolyte combination would be required to produce the PEC *J-E* data observed from the photochemically active area of the integrated n-p$^+$-Si/TiO_2/Ni-island photoelectrode asssembly described here. An analogous calculation indicated that a 12.7% GaAs PV cell would be required to produce the *J-E* behavior observed for the integrated n-p$^+$-GaAs/TiO_2/Ni film photoelectode assembly described here.

The photovoltage produced by the n-Si/TiO_2 interfaces was ~0.4 V, which is lower than that of an np$^+$-Si diode or than the theoretical bulk recombination limit. The photovoltage might be improved by exercising further control over the interface; for example, by initiating ALD with a seed layer of C-Si bonds. Methyl termination passivates the Si surface electronically and introduces interfacial dipoles that can generate high photovoltages (*31*). In addition, the ability to engineer the energy levels and the distribution of defect states in chemically stable coatings such as TiO_2 offers the opportunity to stabilize a host of narrow band-gap semiconductors for use in oxidative photochemistry. We have explored the use of thick pinhole-free ALD-TiO_2 films to protect Si, as well as GaAs and GaP, from photocorrosion. This method suggests a logical extension to other materials such as II-VIs (e.g., CdSe), III-nitrides (e.g., InGaN), and chalcolpyrites (e.g., $CuInGaSe_2$), which opens the possibility for the use of earth-abundant semiconductors other than stable metal oxides for efficient solar fuel production.

REFERENCES AND NOTES

1. N. Lewis, *Electrochem. Soc. Interface* **22**, 43–49 (2013).
2. B. A. Pinaud *et al*., *Energy Environ. Sci.* **6**, 1983–2002 (2013).
3. M. G. Walter *et al*., *Chem. Rev.* **110**, 6446–6473 (2010).
4. M. Pourbaix, *Atlas of Electrochemical Equilibria in Aqueous Solutions* (National Association of Corrosion Engineers, Houston, TX, ed. 2, 1974).
5. J. R. McKone, N. S. Lewis, H. B. Gray, *Chem. Mater.* **26**, 407–414 (2014).
6. S. Hu, C. Xiang, S. Haussener, A. D. Berger, N. S. Lewis, *Energy Environ. Sci.* **6**, 2984–2993 (2013).
7. Y. Nakato, T. Ohnishi, H. Tsubomura, *Chem. Lett.* **3**, 883–886 (1975).
8. R. C. Kainthla, *J. Electrochem. Soc.* **134**, 841–845 (1987).
9. M. J. Kenney *et al*., *Science* **342**, 836–840 (2013).
10. F. R. F. Fan, R. G. Keil, A. J. Bard, *J. Am. Chem. Soc.* **105**, 220–224 (1983).
11. F. Decker, M. Fracastoro-Decker, W. Badawy, K. Doblhofer, H. Gerischer, *J. Electrochem. Soc.* **130**, 2173–2179 (1983).
12. F. Fan, B. Wheeler, A. Bard, R. Noufi, *J. Electrochem. Soc.* **128**, 2042–2045 (1981).
13. N. C. Strandwitz *et al*., *J. Phys. Chem. C* **117**, 4931–4936 (2013).
14. K. Sun *et al*., *Energy Environ. Sci.* **5**, 7872–7877 (2012).
15. Y. W. Chen *et al*., *Nat. Mater.* **10**, 539–544 (2011).
16. A. G. Scheuermann, J. D. Prange, M. Gunji, C. E. D. Chidsey, P. C. McIntyre, *Energy Environ. Sci.* **6**, 2487–2496 (2013).
17. S. Dueñas *et al*., *Semicond. Sci. Technol.* **20**, 1044–1051 (2005).
18. Materials and methods are available as supplementary materials on *Science* Online.
19. Y. Matsumoto, E. Sato, *Mater. Chem. Phys.* **14**, 397–426 (1986).
20. D. A. Corrigan, *J. Electrochem. Soc.* **136**, 723–728 (1989).
21. B. S. Yeo, A. T. Bell, *J. Phys. Chem. C* **116**, 8394–8400 (2012).
22. H. N. Ghosh, J. B. Asbury, Y. Weng, T. Lian, *J. Phys. Chem. B* **102**, 10208–10215 (1998).
23. S. A. Campbell *et al*., *IBM J. Res. Develop.* **43**, 383–392 (1999).
24. B. Kalanyan, G. Parsons, *ECS Trans.* **41**, 285–292 (2011).
25. M. H. Lee *et al*., *Angew. Chem. Int. Ed. Engl.* **51**, 10760–10764 (2012).
26. A. Paracchino, V. Laporte, K. Sivula, M. Grätzel, E. Thimsen, *Nat. Mater.* **10**, 456–461 (2011).
27. B. Seger *et al*., *J. Am. Chem. Soc.* **135**, 1057–1064 (2013).
28. S. Avasthi *et al*., *Appl. Phys. Lett.* **102**, 203901 (2013).
29. C. C. L. McCrory, S. Jung, J. C. Peters, T. F. Jaramillo, *J. Am. Chem. Soc.* **135**, 16977–16987 (2013).
30. M. R. Shaner, K. T. Fountaine, H.-J. Lewerenz, *Appl. Phys. Lett.* **103**, 143905 (2013).
31. R. L. Grimm *et al*., *J. Phys. Chem. C* **116**, 23569–23576 (2012).

ACKNOWLEDGMENTS

This work is supported through the Office of Science of the U.S. Department of Energy (DOE) under award no. DE-SC0004993 to the Joint Center for Artificial Photosynthesis, a DOE Energy Innovation Hub. M.S. acknowledges the Resnick Sustainability Institute for a graduate fellowship, and B.S.B. acknowledges the Beckman Institute at the California Institute of Technology for support. XPS was performed at the Molecular Materials Research Center in the Beckman Institute at the California Institute of Technology. TEM imaging and spectroscopy were performed at the Center for Electron Microscopy and Microanalysis, University of Southern California. We thank H.- J. Lewerenz, C. Koval, and F. Houle for fruitful discussions; Y. Guan for secondary-ion mass spectrometry measurements; S. R. Nutt for use of the microscopy and microanalysis facility; P. D. Dapkus for the use of the metal-organic chemical vapor deposition facility; S. Ardo for help in boron-diffusion doping; and K. Papadantonakis for assistance with editing this manuscript. The authors' institution (California Institute of Technology) has filed a provisional U.S. patent application directly relating to the work described in the paper (patent application no. 61/889,430, filed on 10 October 2013).

SUPPLEMENTARY MATERIALS

www.sciencemag.org/content/344/6187/1005/suppl/DC1
Materials and Methods
Supplementary Text
Figs. S1 to S17
References (*32*, *33*)

28 January 2014; accepted 1 May 2014
10.1126/science.1251428

WATER STRUCTURE

Vibrational spectral signature of the proton defect in the three-dimensional $H^+(H_2O)_{21}$ cluster

Joseph A. Fournier, Christopher J. Johnson, Conrad T. Wolke, Gary H. Weddle, Arron B. Wolk, Mark A. Johnson*

The way in which a three-dimensional network of water molecules accommodates an excess proton is hard to discern from the broad vibrational spectra of dilute acids. The sharper bands displayed by cold gas-phase clusters, $H^+(H_2O)_n$, are therefore useful because they encode the network-dependent speciation of the proton defect and yet are small enough to be accurately treated with electronic structure theory. We identified the previously elusive spectral signature of the proton defect in the three-dimensional cage structure adopted by the particularly stable $H^+(H_2O)_{21}$ cluster. Cryogenically cooling the ion and tagging it with loosely bound deuterium (D_2) enabled detection of its vibrational spectrum over the 600 to 4000 cm^{-1} range. The excess charge is consistent with a tricoordinated H_3O^+ moiety embedded on the surface of a clathrate-like cage.

The nature of proton speciation in water remains an elusive aspect of aqueous chemistry because of the remarkably diffuse vibrational features traceable to the excess proton in dilute acid solutions (*1*–*3*). The spectroscopic properties of small protonated water clusters, $H^+(H_2O)_n$, frozen into well-defined structures, have therefore attracted a great deal of interest over the past decade, as they reveal how the spectral signatures associated

Sterling Chemistry Laboratory, Yale University, New Haven, CT 06520, USA.
*Corresponding author. E-mail: mark.johnson@yale.edu

Amorphous TiO_2 coatings stabilize Si, GaAs, and GaP photoanodes for efficient water oxidation
Shu Hu, Matthew R. Shaner, Joseph A. Beardslee, Michael Lichterman, Bruce S. Brunschwig and Nathan S. Lewis (May 29, 2014)
Science **344** (6187), 1005-1009. [doi: 10.1126/science.1251428]

Editor's Summary

Keeping semiconductors safe from harm

Solar cells harvest the energy of sunlight to create electricity, but electricity is hard to store. Solar cells could also be used to make hydrogen from water, which can be stored as a fuel. Separating water into hydrogen and oxygen, however, presents challenges, especially if this is done directly by illuminating the anode that oxides water. Under the acidic or alkaline conditions needed for practical devices, semiconducting anode materials corrode during operation. Hu *et al.* now show that amorphous titanium dioxide coatings can protect semiconductors from alkaline corrosion while still allowing light through.

Science, this issue p. 1005
